RAPID COMMUNICATION

Magnetic Resonance in Medicine 00:00–00 (2017)

Simultaneous Multislice Imaging for Native Myocardial T_1 Mapping: Improved Spatial Coverage in a Single Breath-Hold

Sebastian Weingärtner,[1,2,3]* Steen Moeller,[2] Sebastian Schmitter,[2,4] Edward Auerbach,[2] Peter Kellman,[5] Chetan Shenoy,[6] and Mehmet Akçakaya[1,2]

Purpose: To develop a saturation recovery myocardial T_1 mapping method for the simultaneous multislice acquisition of three slices.

Methods: Saturation pulse-prepared heart rate independent inversion recovery (SAPPHIRE) T_1 mapping was implemented with simultaneous multislice imaging using FLASH readouts for faster coverage of the myocardium. Controlled aliasing in parallel imaging (CAIPI) was used to achieve minimal noise amplification in three slices. Multiband reconstruction was performed using three linear reconstruction methods: Slice- and in-plane GRAPPA, CG-SENSE, and Tikhonov-regularized CG-SENSE. Accuracy, spatial variability, and interslice leakage were compared with single-band T_1 mapping in a phantom and in six healthy subjects.

Results: Multiband phantom T_1 times showed good agreement with single-band T_1 mapping for all three reconstruction methods (normalized root mean square error $<1.0\%$). The increase in spatial variability compared with single-band imaging was lowest for GRAPPA (1.29-fold), with higher penalties for Tikhonov-regularized CG-SENSE (1.47-fold) and CG-SENSE (1.52-fold). In vivo multiband T_1 times showed no significant difference compared with single-band (T_1 time $\pm$ intersegmental variability: single-band, 1580 ± 119 ms; GRAPPA, 1572 ± 145 ms; CG-SENSE, 1579 ± 159 ms; Tikhonov, 1586 ± 150 ms [analysis of variance; $P = 0.86$]). Interslice leakage was smallest for GRAPPA (5.4%) and higher for CG-SENSE (6.2%) and Tikhonov-regularized CG-SENSE (7.9%).

Conclusion: Multiband accelerated myocardial T_1 mapping demonstrated the potential for single–breath-hold T_1 quantification in 16 American Heart Association segments over three slices. A 1.2- to 1.4-fold higher in vivo spatial variability was observed, where GRAPPA-based reconstruction showed the highest homogeneity and the least interslice leakage. **Magn Reson Med 000:000–000, 2017. © 2017 International Society for Magnetic Resonance in Medicine.**

Key words: myocardial T_1 mapping; simultaneous multislice imaging; multiband; saturation recovery; SAPPHIRE

INTRODUCTION

Quantitative imaging of the heart using MRI has recently emerged to a major focus area within the cardiac MRI community. The quantification of various relaxation parameters [T_1 (1,2), $T_{1\rho}$ (3,4), T_2 (5–7), T_2^* (8,9)] has revealed clinical sensitivity to a wide range of ischemic and nonischemic cardiomyopathies (10–12). In particular, the spatially resolved assessment of the longitudinal relaxation time T_1 (referred to as T_1 mapping) shows promising potential to enhance quality of cardiac MRI for prognosis and diagnosis of cardiomyopathies (13).

Parameter maps of the myocardium are commonly obtained from a series of single-shot images with different contrast weightings, all of which are acquired during a single breath-hold. Three-slice coverage in short axis orientation is recommended for evaluation because it captures the heterogeneity across the left ventricle better than single-slice acquisitions (14). Conventional myocardial T_1 mapping methods acquire only a single slice per breath-hold, necessitating rest periods between subsequent breath-holds, leading to patient discomfort and long scan times. Furthermore, repeated breath-holds may compromise image registration (15–18).

Free-breathing T_1 mapping methods have been proposed to improve patient comfort and enable increased spatial resolution or coverage. In these techniques, respiratory motion compensation may be performed via prospective triggering (19) or gating based on diaphragmatic image navigators (20–22), retrospective self-gating (23,24), or prospective slice tracking (25). However, respiratory gating and triggering lead to increased scan times, whereas tracking potentially induces blurring in the presence of heavy breathing. Consequently, a fast single breath-hold acquisition is the preferred approach.

Image acceleration techniques, such as parallel imaging, are frequently used in breath-held myocardial T_1

[1]Electrical and Computer Engineering, University of Minnesota, Minneapolis, Minnesota, USA.

[2]Center for Magnetic Resonance Research, University of Minnesota, Minneapolis, Minnesota, USA.

[3]Computer Assisted Clinical Medicine, University Medical Center Mannheim, Heidelberg University, Mannheim, Germany.

[4]Medical Physics and Metrological Information Technology, Physikalisch-Technische Bundesanstalt, Berlin, Germany.

[5]National Heart, Lung, and Blood Institute, National Institutes of Health, Bethesda, Maryland, USA.

[6]Cardiovascular Division, Department of Medicine, University of Minnesota, Minneapolis, Minnesota, USA.

Grant sponsor: National Institutes of Health; Grant numbers: R00HL111410, P41EB015894.

*Correspondence to: Sebastian Weingärtner, Ph.D., Electrical and Computer Engineering, University of Minnesota, 200 Union Street SE, Minneapolis, MN 55455. E-mail: sweingae@umn.edu

Sebastian Weingärtner and Mehmet Akçakaya are inventors of a pending US and European patent entitled "Methods for scar imaging in patients with arrhythmia" that describes the SAPPHIRE imaging sequence.

Received 14 December 2016; revised 10 April 2017; accepted 6 May 2017

DOI 10.1002/mrm.26770

Published online 00 Month 2017 in Wiley Online Library (wileyonlinelibrary.com).

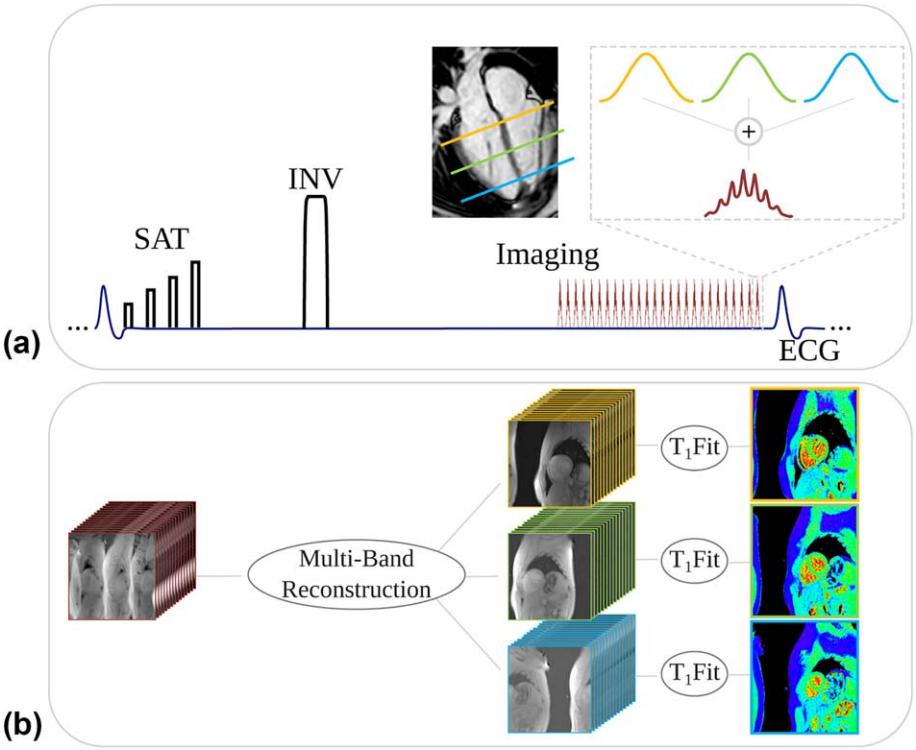

FIG. 1. (**a**) Schematic description of the MB T_1 mapping sequence. (**b**) Reconstruction pipeline. A SAPPHIRE sequence with combined saturation/inversion recovery preparation is combined with a FLASH imaging readout. The MB excitation pulses are obtained as the sum of three sinc SB excitations at different frequency bands. Image reconstruction is performed to unalias the MB slices and the in-plane undersampling, with subsequent phase-sensitive fitting of the saturation/inversion recovery curve to obtain quantitative T_1 maps.

mapping to provide sufficient spatial resolution in the single-shot acquisitions during the brief diastolic quiescence (14). Compressed sensing has also been used to improve spatial resolution in T_1 mapping in a single breath-hold (26,27). However, these approaches, as commonly used, do not affect the coverage or the total acquisition time and thus do not change the breath-hold duration.

Simultaneous multislice (SMS) or multiband (MB) imaging is an alternative acceleration technique for acquiring multiple slices simultaneously (28), where the only SNR reduction compared with single-slice imaging is due to coil geometry (29). In MB imaging, the simultaneous excitation of multiple slices is achieved by playing an excitation pulse, which is obtained as the sum of pulses at different resonance frequencies, corresponding to different slice locations (30). To decrease the noise amplification from unaliasing, better encoding has been proposed with controlled aliasing in volumetric parallel imaging (CAIPIRINHA) (29). Here, cyclic phase shifts, or equivalently a sheared undersampling pattern, is used to induce a shifted object position benefitting 3D and 2D SMS unaliasing (31).

MB imaging has become a popular tool in neurological applications (32); however, its use in cardiac applications has been limited, due to unfavorable coil geometries used in body imaging. MB imaging has been used in myocardial perfusion imaging with a 2-fold MB and 2.5-fold in-plane acceleration (33), as well as 3- to 5-fold MB and no in-plane acceleration (34). Cardiac cine imaging with 2-fold MB and 3-fold in-plane acceleration at 3T (35) and with 2- to 3-fold MB and 2- to 4-fold in-plane acceleration at 7T (36) have also been investigated. However, its effect on myocardial MR parameter quantification and precision has not been explored.

In this study, we sought to evaluate the potential of MB imaging to accelerate myocardial T_1 mapping and to enable 16-segment quantification in a single breath-hold. A saturation pulse-prepared heart rate independent inversion recovery (SAPPHIRE) sequence with CAIPIRINHA-MB accelerated FLASH imaging was proposed for the simultaneous acquisition of three slices. T_1 time accuracy and precision were compared with conventional single-band (SB) SAPPHIRE imaging in phantom scans. In vivo results were presented for native T_1 mapping in healthy subjects.

METHODS

Sequence

Figure 1a depicts the schematic of the proposed pulse sequence. Combined sinc excitation pulses (bandwidth time product = 2.0; pulse duration = 1.0 ms) at three frequencies were employed for MB excitation in the FLASH imaging readout of a SAPPHIRE (37) sequence, using hybrid saturation/inversion preparation for T_1 sensitization. Fifteen images with different inversion times were acquired during a single breath-hold. All inversion times are confined to a single heartbeat, resulting in an acquisition over 15 heartbeats. The inversion times are linearly distributed between the minimal inversion time (185 ms in this study) and the maximum inversion time, determined by the start of the diastolic phase. For phantom imaging, the maximum inversion time was selected as 760 ms, corresponding to a heart rate of 60 beats per minute. Pulse phases of the three base excitation pulses were cycled with a phase increment of $2\pi/3$ from slice to slice to achieve a field of view (FOV) shift of 1/3 in the images between adjacent slices. Additionally, a constant slice-specific phase shift was added to each individual pulse

phase, previously optimized to minimize peak B_1^* amplitude to reduce SAR burden of the sequence (38,39).

All MB and SB T_1 mapping were performed at 3T with a single-shot electrocardiography (ECG)-triggered FLASH sequence with the following imaging parameters: uniform in-plane undersampling = 2; FOV = $320 \times 320\,mm^2$; spatial resolution = $2.0 \times 2.1\,mm^2$; slice thickness = 10 mm; slice gap = 10 mm; partial Fourier = 6/8; number of phase-encode lines = 69; repetition time = 4.0 ms; echo time = 2.0 ms; flip angle = 10°; bandwidth = 505 Hz/pixel; linear k-space ordering; inversion pulse: tan/tanh adiabatic full passage, 2.56 ms (40); saturation pulse: four compartment Water Suppression Enhanced through T_1 effect (WET) module (41). 24 reference lines were acquired in the k-space center for each image.

To enable the reconstructions for slice unaliasing, a 1-second reference scan was used to acquire low-resolution images of three slices, during free-breathing and without ECG-gating (FOV = $320 \times 320\,mm^2$; spatial resolution = $2 \times 5\,mm^2$; slice thickness = 10 mm, repetition time = 3.6 ms; echo time = 1.8 ms; flip angle = 10°; bandwidth = 500 Hz/pixel). For comparison, an additional three-heartbeat reference scan with the same parameters was also acquired with end-diastolic ECG triggering and breath-holding.

Reconstruction

The acquired raw data with MB aliasing and in-plane acceleration were exported from the scanner, and the T_1-weighted images were reconstructed offline in MATLAB (MathWorks, Natick, Massachusetts, USA) using three different linear reconstruction approaches:

1. Multislice unaliasing performed using slice-GRAPPA (42), followed by in-plane GRAPPA (43), whose kernels were calibrated from the low resolution reference scan, with (5,5) and (4,5) kernel sizes, respectively. The final images were generated using a coil sensitivity–weighted combination of the individual coil images.
2. CG-SENSE (44) reconstruction for slice and in-plane unaliasing. CG-SENSE was used instead of SENSE to use the signal from the fully sampled MB-encoded k-space center. Coil sensitivity maps for each band and each coil were generated from the reference scan.
3. CG-SENSE reconstruction with additional Tikhonov regularization (45). A separate sub-study, detailed in Supporting Information S1 and Supporting Figure S1, was performed to empirically optimize the Tikhonov regularization parameter as 0.05.

For each of the three methods, following the MB slice and in-plane unaliasing, phase-sensitive fitting, as proposed for inversion recovery T_1 mapping (15) was performed on the final T_1-weighted images to obtain T_1 maps (Fig. 1b).

Phantom Imaging

All imaging was performed using a 3T Siemens Magnetom Prisma (Siemens Healthcare, Erlangen, Germany) system with a 30-channel receiver coil array.

Phantom imaging for T_1 quantification accuracy and precision was performed using SB and MB SAPPHIRE in a cylindrical phantom containing multiple spherical compartments of gadolinium or sucrose-doped agarose gel, with T_1 and T_2 times in the in vivo range [T_1 = 200–2500 ms; T_2 = 50–250 ms (46)]. All scans were performed with 10 repetitions to allow assessment of noise-dependent variation.

In Vivo Imaging

The study was approved by our institutional review board, and written informed consent was acquired before each examination. Imaging was performed in six healthy subjects (three men and three women; mean age, 36 ± 16 years) with no contraindications to MRI. Native T_1 maps were acquired using conventional SB and the proposed MB SAPPHIRE in these short-axis slices. Conventional SB SAPPHIRE was performed in three breath-holds for coverage of the three slices. MB SAPPHIRE images of matching slices were acquired in a single breath-hold. Free-breathing and breath-hold calibration scans were acquired before the MB acquisition.

Data Analysis

Phantom accuracy was defined as the deviation of the average T_1 time within manually drawn regions of interest (ROIs), averaged over all repetitions. Spatial variability was assessed as the standard deviation across the ROI in the homogenous phantom vials, averaged over all repetitions.

Leakage analysis was performed using the respective MB reconstruction on spatially shifted SB acquisitions (31). The three slices from the SB acquisitions, corresponding to no saturation preparation, were shifted to match the FOV shifts of the MB acquisition. Then, each of these shifted slices were run through the three separate reconstruction algorithms, using the kernels/coil sensitivity maps as generated from the respective reference scans. Ideally, this leads to only the original input slice being reconstructed, with no signal content in the other two slices. Thus, the leakage was defined as the resulting residual signal in the two non-input slices. This was repeated for the other two shifted SB slices. Using the linearity of the reconstructions, the total leakage in each slice was generated by addition of the leakages from the three shifted SB slices as inputs.

In vivo T_1 and leakage maps were evaluated in manually drawn ROIs, delineating the endo- and epicardial contours while carefully avoiding areas of partial voluming. Quantitative comparison of the T_1 times and T_1 time spatial variability was performed according to the American Heart Association (AHA) 16-segment model (47). In vivo T_1 time spatial variability was defined as the inter-segment variation.

Statistical differences in the T_1 times, and interslice leakage were assessed using one-way analysis of variance (ANOVA) with subsequent paired Student *t* tests. Kruskal-Wallis group analysis and Wilcoxon signed rank tests were used to statistically compare the spatial variability of T_1 times. P values < 0.05 were considered to be significant for group tests, and Bonferroni correction was

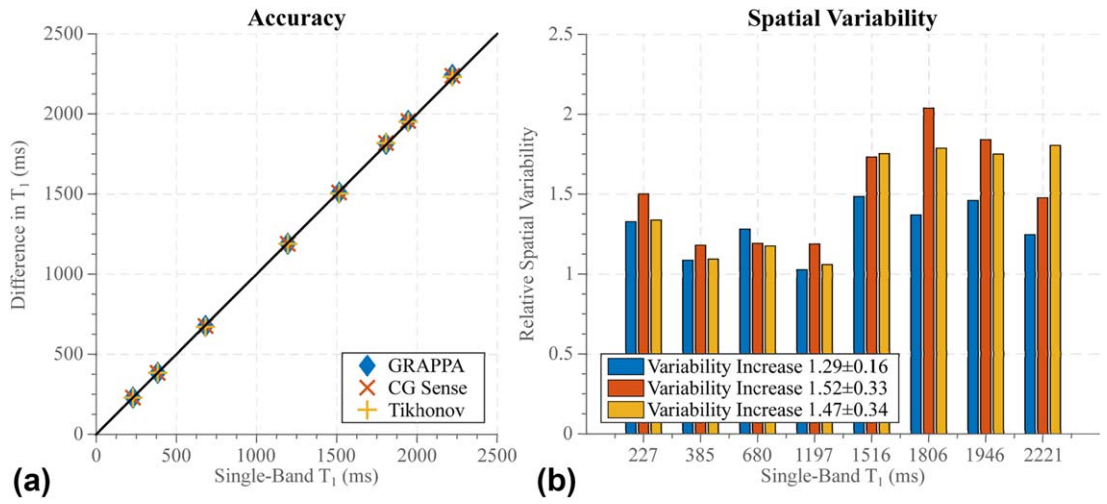

FIG. 2. Phantom results depicting the accuracy (**a**) and spatial variability (**b**) of the proposed technique in comparison with conventional SB imaging for three different linear reconstruction methods. The MB T_1 times show good agreement with the SB acquisition. A 1.3- to 1.5-fold increase of noise variability is shown with the different MB reconstruction techniques compared with SB imaging.

applied for pairwise tests with significance levels of 0.0083 for T_1 time and spatial variability comparison (six tests) and 0.017 for leakage analysis (three tests).

RESULTS

Phantom Imaging

Figure 2 depicts the results of phantom imaging, showing good agreement between SB T_1 mapping and all MB reconstruction methods, with minor differences between the three reconstruction techniques (normalized root mean square error: GRAPPA, 0.62%; CG-SENSE, 0.66%; Tikhonov-regularized CG-SENSE, 0.59%). Spatial variability in the homogeneous T_1 phantom shows the highest increase for the nonregularized CG-SENSE reconstruction and only minor changes for GRAPPA (variability relative to single-band T_1 mapping: GRAPPA, 1.29 ± 0.16; CG-SENSE, 1.52 ± 0.33; Tikhonov-regularized CG-SENSE, 1.47 ± 0.34).

In Vivo Imaging

Figure 3 shows representative T_1 maps acquired in two subjects with SB and MB SAPPHIRE, using the free-breathing calibration scan. All volunteer scans are shown

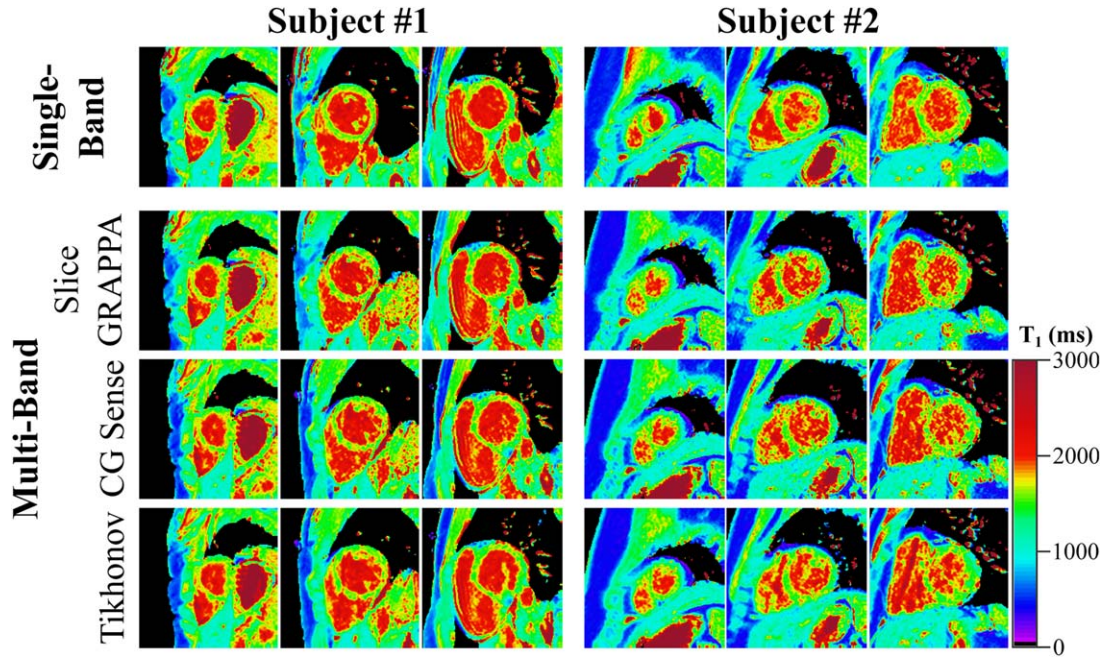

FIG. 3. Representative T_1 maps from two subjects, comparing an MB acquisition with various linear reconstructions with conventional SB T_1 mapping. Increased heterogeneity of the T_1 times is observed using conventional CG-SENSE, compared with SB T_1 mapping. GRAPPA and Tikhonov-regularized MB imaging achieves image quality that is visually comparable to SB imaging, although Tikhonov-regularized CG-SENSE displayed increased interslice leakage, as apparent in subject #1.

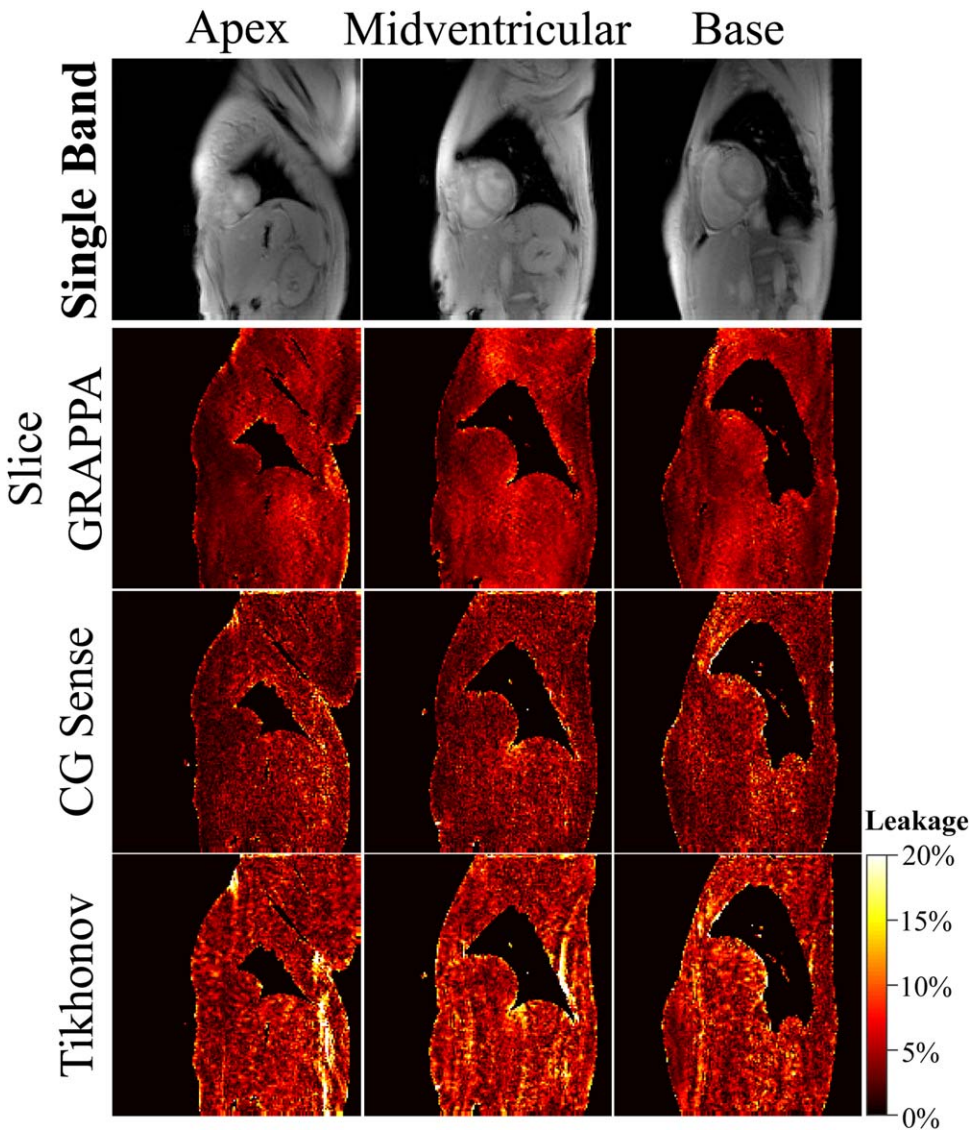

FIG. 4. Leakage maps comparing three MB reconstructions. The top row presents the corresponding SB images with no magnetization preparation, as used to generate the leakage maps. GRAPPA shows mild and noise-like leakage across the FOV. Slightly decreased leakage, albeit with increased intensity hot spots is depicted for CG-SENSE. Tikhonov-regularized CG-SENSE displays the highest interslice leakage of the three methods, though the intensity hot spots lie predominantly outside the myocardium.

in Supporting Figure S2. Conventional SB acquisition produces visually homogeneous T_1 maps (T_1 time ± spatial variability: subject #1, 1572 ± 95 ms; subject #2, 1546 ± 126 ms). For the MB T_1 scans, reconstruction with slice GRAPPA resulted in the least amount of spatial variability (subject #1, 1567 ± 111 ms; subject #2, 1563 ± 139 ms), providing images that are visually comparable to SB imaging. Tikhonov-regularized CG-SENSE also provided images with comparable quality, although with slightly increased spatial variability (subject #1, 1567 ± 112 ms; subject #2: 1583 ± 155 ms). CG-SENSE showed the strongest increase in spatial variability (subject #1, 1563 ± 118 ms; subject #2, 1593 ± 170 ms). On visual inspection, CG-SENSE–based reconstructions showed higher leakage, especially in the basal slice, whereas less leakage was observed for slice GRAPPA. The same trend is observed in the leakage maps of the three reconstruction techniques (Fig. 4): Leakage using GRAPPA reconstruction appears visually homogeneous and noise-like. Increased structure but reduced noise-like variation can be observed using CG-SENSE, while the highest leakage is observed with regularized CG-SENSE.

Bullseye representations of the quantitative evaluation of myocardial T_1 times, in vivo spatial variability and interslice leakage for MB and SB T_1 mapping across all subjects in the 16 AHA segments are depicted in Figure 5. For MB acquisitions, all reconstruction techniques result in T_1 values comparable to the SB reference (ANOVA; $P = 0.86$). As in phantom scans, the increase in spatial variability is the least for GRAPPA, followed by Tikhonov-regularized CG-SENSE and CG-SENSE (Kruskal-Wallis $P = 0.07$, pair-wise $P \leq 0.031$, except for GRAPPA versus Tikhonov-regularized CG-SENSE $P = 0.44$ and CG-SENSE versus Tikhonov-regularized CG-SENSE $P = 0.094$). However, the Tikhonov-regularized reconstruction also shows the highest interslice leakage, particularly in segments 2, 5, and 6 of the basal slice. GRAPPA showed the most uniform leakage performance across segments with the smallest mean (Kruskal-Wallis $P = 0.22$; GRAPPA versus Tikhonov-regularized CG-SENSE $P = 0.25$, GRAPPA versus CG-SENSE $P = 0.031$, CG-SENSE versus Tikhonov-regularized CG-SENSE $P = 0.031$).

The same trend can be observed in blood T_1 times. No significant difference was found between SB and the three

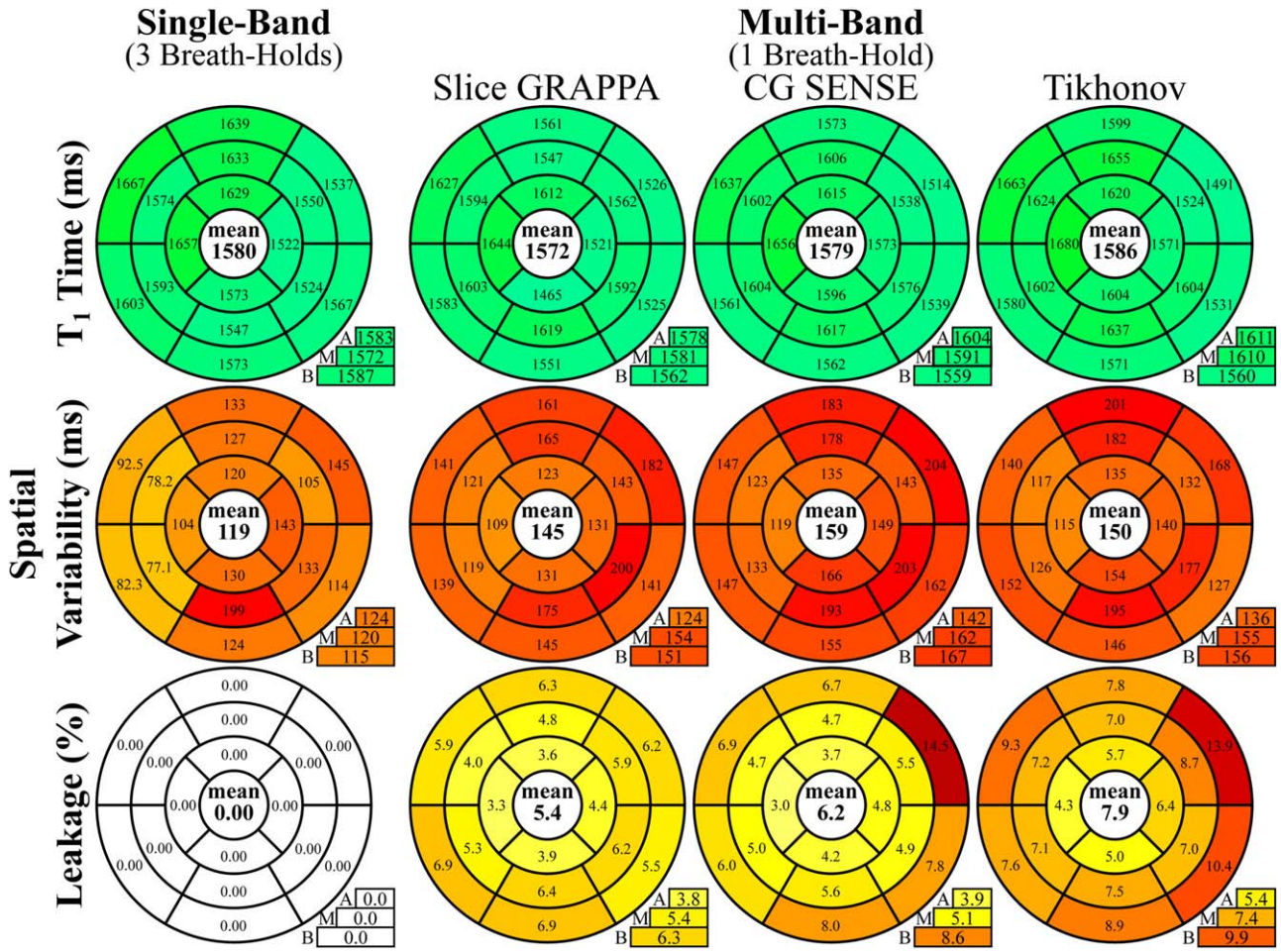

FIG. 5. Bullseye representation of myocardial T_1 times, T_1 time spatial variability, and interslice leakage, as quantitatively analyzed according to the AHA 16-segment model. All three reconstruction methods show T_1 times comparable to SB imaging, though with increased intrasegment variability. Slice GRAPPA shows the smallest increase in spatial variability compared with SB T_1 mapping and the smallest interslice leakage.

MB reconstructions (ANOVA, $P = 0.98$; SB, 2043 ± 80 ms; GRAPPA, 2034 ± 71 ms; CG-SENSE, 2042 ± 94 ms; Tikhonov-regularized CG-SENSE, 2026 ± 93 ms). Blood T_1 time spatial variability was 1.3- to 1.6-fold higher using MB compared with SB T_1 mapping, but differences were not found to be significant (Kruskal-Wallis $P = 0.102$; SB, 130 ± 13 ms; GRAPPA, 170 ± 31 ms; CG-SENSE, 206 ± 82 ms; Tikhonov-regularized CG-SENSE, 172 ± 51 ms).

In our study, no visual difference was observed when performing the MB reconstructions using the free-breathing versus breath-held calibration scans. T_1 maps reconstructed with GRAPPA using the different types of calibration data are depicted in Figure 6. There were no significant differences among the T_1 values ($P > 0.57$) or the spatial variability ($P > 0.59$) for the two types of calibration data. GRAPPA displayed the highest amount of resilience to changes in the calibration data (relative difference: T_1, $0.015 \pm 0.269\%$; variability, $0.223 \pm 2.28\%$). CG-SENSE reconstructions showed a slight but nonsignificant trend of increased variability with the free-breathing calibration data (relative difference CG-SENSE: T_1, $-0.472 \pm 1.03\%$; variability, $-7.82 \pm 11.9\%$; relative difference Tikhonov-regularized CG-SENSE: T_1, $-0.517 \pm 0.994\%$; variability, $-3.62 \pm 7.19\%$).

DISCUSSION

In this study, we evaluated an MB imaging sequence for accelerated myocardial T_1 mapping that enables 16-segment quantification in a single breath-hold. We evaluated three linear reconstruction algorithms for unaliasing the MB data and their effect on T_1 estimation and spatial variability. Phantom and in vivo experiments revealed that all three methods showed comparable accuracy to conventional single-band imaging, albeit at 1.2- to 1.4-fold loss in spatial variability.

MB imaging suffers from decreased SNR due to unfavorable coil geometry in cardiac applications. Our results show that a combination of slice and in-plane GRAPPA showed the least noise amplification, with the least amount of interslice leakage and a uniform leakage profile across all the myocardial segments. Among the SENSE-based reconstructions, Tikhonov regularization reduced the effects of noise amplification. However, it also increased the interslice leakage, albeit most of the increased leakage being evident outside the heart, with the exception of some basal segments. Nonlinear reconstruction techniques with appropriate regularization can also be used for further removal of artifacts due to noise

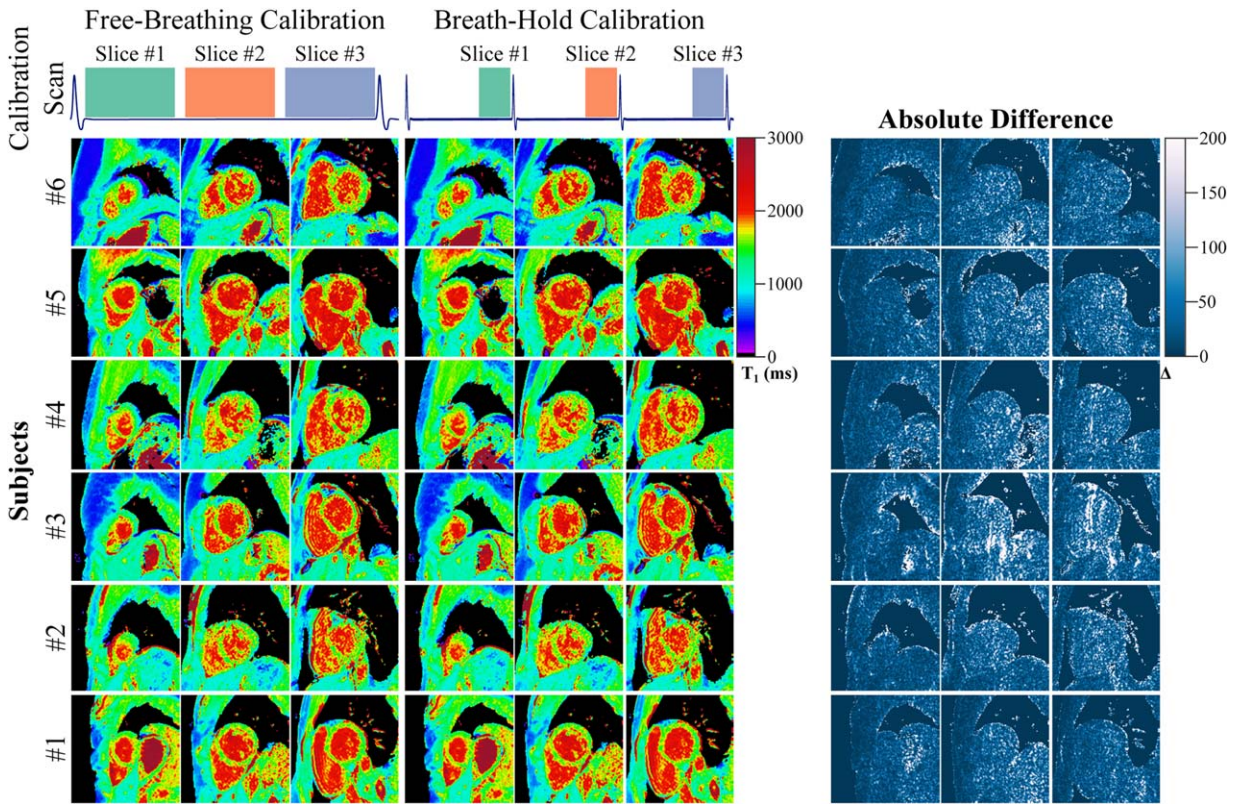

FIG. 6. MB T_1 maps reconstructed with slice GRAPPA using free-breathing or breath-hold calibration data. The acquisition scheme for the calibration data is depicted in the top row. Images of six healthy subjects are presented below, along with the corresponding difference maps. MB T_1 maps with both calibration data are of similar quality and differences are barely noticeable on visual assessment. Difference maps reveal minor noise-like changes when using a differently acquired calibration data set.

and leakage. However, these were not explored in the current study in order to provide a uniform comparison of spatial variability and leakage for the linear reconstruction techniques.

The position of the heart is known to show major variations between separate breath-holds even in healthy volunteers. Hence, T_1 map acquisition of three short-axis slices in separate breath-holds provides potentially nonequidistant coverage with bias toward basal or apical T_1 times. Because all slices are acquired simultaneously in MB T_1 mapping, equidistant and uniform coverage of the left ventricle is ensured in a short-axis stack scan with the proposed technique.

In this study, MB reconstructions, in particular slice GRAPPA, were observed to be resilient to interscan motion between the calibration and the measurement data. This result is encouraging for the applicability of SMS imaging to cardiac applications, where potential mismatches in cardiac or respiratory phases might be unavoidable. The use of calibration scans without cardiac or respiratory gating is advantageous, as additional scan time requirements are minimized. Further studies are needed to verify this trend in other cardiac MR applications.

Myocardial T_1 mapping is most commonly performed using balanced Steady-State Free Precession (bSSFP) imaging readouts, which are less disruptive to the longitudinal magnetization recovery curve (48). Recently, the use of FLASH imaging has been explored for inversion recovery–based T_1 mapping (49,50). Saturation recovery T_1 mapping methods are known to allow for accurate T_1 quantification with FLASH imaging readout (51). Accordingly T_1 times assessed with FLASH SAPPHIRE in healthy subjects are in good agreement with a recent study of steady-state–free precession-based saturation recovery T_1 mapping at 3T (41). FLASH imaging has been proven to be beneficial at 3T due to its resilience against off-resonance artifacts, which might be a major disruptive factor to bSSFP image quality at high field strengths. However, in T_1 mapping, this comes at the cost of reduced noise resilience and increased end-diastolic imaging times. Due to the linear k-space ordering, and because border zones are commonly excluded when evaluating myocardial T_1 maps, the increase in acquisition window duration caused by the long FLASH repetition time has been reported previously to not be an issue at 1.5T (52). Nonetheless, the repetition time of the FLASH sequence can be shortened further by optimizing spoiling strategies or increasing imaging bandwidth as a trade-off against T_1 mapping precision. For MB imaging, FLASH has the additional advantage that MB phase cycling can be encoded in the radiofrequency phase of each band, rather than using encoding gradients as for EPI or SSFP imaging, which might introduce additional signal loss due to in-band dephasing (53).

To mitigate the reduced baseline SNR of FLASH imaging, T_1 maps were acquired over 15 heartbeats, in contrast to previous bSSFP-based SAPPHIRE protocols, which use nine to 11 images (37,41,54,55). The longer breath-hold duration was not disruptive in the study cohort. However, in critically ill patients or patients with respiratory restrictions, reduced sequence duration can be achieved at a trade-off against a slight loss in precision.

Although MB T_1 mapping was demonstrated with a SAPPHIRE saturation recovery sequence design, this acceleration technique can be applied straightforwardly to other saturation recovery techniques, such as saturation recovery single-shot acquisition (SASHA) (56). In this study, we chose SAPPHIRE instead of SASHA because of recent results showing that SAPPHIRE is more artifact resilient and more precise (41,54). The technique may also be applied to myocardial T_1 mapping where the T_1 recovery curve spans several heartbeats, such as the modified Look-Locker inversion recovery technique and its variants (48,57,58). However, progressive saturation of the blood in several slices simultaneously might lead to diminished signal from the blood pool over time, especially at high MB factors. Furthermore, the FLASH imaging readouts as used in the proposed MB acquisition substantially compromise the accuracy in commonly used inversion recovery T_1 mapping sequences. Although tailored reconstruction schemes have been proposed to mitigate this effect (59), MB inversion recovery T_1 mapping is beyond the scope of this study, but this method warrants further investigation.

All SAPPHIRE T_1 maps in the current study were reconstructed using curve fitting to phase-sensitive data. This approach has previously been proposed for inversion recovery T_1 mapping (15), resulting in reduced in vivo variability, because it eliminates the necessity to restore the signal polarity along the inversion recovery curve. Furthermore, a Gaussian noise characteristic is maintained, potentially increasing T_1 mapping accuracy, when least-squares fitting is used with low baseline SNR or when the T_1-weighted myocardial signal falls close to the zero crossing. These advantages of phase-sensitive T_1 mapping can also be harvested in hybrid SAPPHIRE T_1 mapping, because the dynamic range spans across both the positive and negative longitudinal magnetizations.

In this study, in vivo imaging was performed during breath-holding. However, in some patients, end-expiration breath-holding cannot be maintained even for short durations. In these cases, respiratory drift may corrupt the T_1 map quality and precision. Dedicated image registration algorithms have been proposed to closely realign the T_1-weighted baseline images, despite the substantial contrast variations (16,17). Although no significant motion-induced artifacts have been observed in our healthy cohort study, such registration techniques can be applied to MB T_1 mapping. Additionally, due to the simultaneous acquisition of multiple slices, similar motion can be expected and simultaneous registration of all three slices may be performed. This may help to reduce the dimensionality of the registration problem and improve the realignment of the baseline images after processing. Potential synergies of image registration and MB cardiac imaging will be explored in future studies.

This study has several limitations. Only a limited number of healthy subjects were included in this proof-of-concept study. Clinical evaluation of single breath-hold whole-heart T_1 mapping in larger cohorts exhibiting specific pathologies is warranted. Because the excitation bands in MB imaging have to be parallel, T_1 maps have only been evaluated in a short axis to allow for the 16-segment analysis. Only a single MB acceleration factor of 3 was studied to allow for T_1 mapping in a single breath-hold, in accordance with the coverage requirements of the Society for Cardiovascular Magnetic Resonance's T_1 mapping task force consensus statement (14).

In conclusion, the proposed technique enables acquisition of native myocardial T_1 maps with improved spatial coverage, allowing for the quantification of the 16 AHA segments over three slices in a single breath-hold. More than 3-fold savings in acquisition time is achieved in young healthy volunteers, at an increased T_1 spatial variability of 1.2- to 1.4-fold using a linear slice GRAPPA reconstruction.

REFERENCES

1. Kellman P, Hansen MS. T1-mapping in the heart: accuracy and precision. J Cardiovasc Magn Reson 2014;16:2.
2. Burt JR, Zimmerman SL, Kamel IR, Halushka M, Bluemke DA. Myocardial T1 mapping: techniques and potential applications. Radiographics 2014;34:377–395.
3. van Oorschot JW, Visser F, Eikendal AL, Vonken EJ, Luijten PR, Chamuleau SA, Leiner T, Zwanenburg JJ. Single breath-hold T1rho-mapping of the heart for endogenous assessment of myocardial fibrosis. Invest Radiol 2016;51:505–512.
4. Muthupillai R, Flamm SD, Wilson JM, Pettigrew RI, Dixon WT. Acute myocardial infarction: tissue characterization with T1rho-weighted MR imaging—initial experience. Radiology 2004;232:606–610.
5. He T, Gatehouse PD, Anderson LJ, Tanner M, Keegan J, Pennell DJ, Firmin DN. Development of a novel optimized breathhold technique for myocardial T2 measurement in thalassemia. J Magn Reson Imaging 2006;24:580–585.
6. Giri S, Chung YC, Merchant A, Mihai G, Rajagopalan S, Raman SV, Simonetti OP. T2 quantification for improved detection of myocardial edema. J Cardiovasc Magn Reson 2009;11:56.
7. Huang TY, Liu YJ, Stemmer A, Poncelet BP. T2 measurement of the human myocardium using a T2-prepared transient-state TrueFISP sequence. Magn Reson Med 2007;57:960–966.
8. Westwood M, Anderson LJ, Firmin DN, Gatehouse PD, Charrier CC, Wonke B, Pennell DJ. A single breath-hold multiecho T2* cardiovascular magnetic resonance technique for diagnosis of myocardial iron overload. J Magn Reson Imaging 2003;18:33–39.
9. Sandino CM, Kellman P, Arai AE, Hansen MS, Xue H. Myocardial T2* mapping: influence of noise on accuracy and precision. J Cardiovasc Magn Reson 2015;17:7.
10. Salerno M, Kramer CM. Advances in parametric mapping with CMR imaging. JACC Cardiovasc Imaging 2013;6:806–822.
11. Hamlin SA, Henry TS, Little BP, Lerakis S, Stillman AE. Mapping the future of cardiac MR imaging: case-based review of T1 and T2 mapping techniques. Radiographics 2014;34:1594–1611.
12. Han Y, Liimatainen T, Gorman RC, Witschey WR. Assessing myocardial disease using T1rho MRI. Curr Cardiovasc Imaging Rep 2014;7:9248.
13. Schelbert EB, Messroghli DR. State of the art: clinical applications of cardiac T1 mapping. Radiology 2016;278:658–676.
14. Moon JC, Messroghli DR, Kellman P, et al.. Myocardial T1 mapping and extracellular volume quantification: a Society for Cardiovascular Magnetic Resonance (SCMR) and CMR Working Group of the European Society of Cardiology consensus statement. J Cardiovasc Magn Reson 2013;15:92.

15. Xue H, Greiser A, Zuehlsdorff S, Jolly MP, Guehring J, Arai AE, Kellman P. Phase-sensitive inversion recovery for myocardial T1 mapping with motion correction and parametric fitting. Magn Reson Med 2013;69:1408–1420.
16. Xue H, Shah S, Greiser A, Guetter C, Littmann A, Jolly MP, Arai AE, Zuehlsdorff S, Guehring J, Kellman P. Motion correction for myocardial T1 mapping using image registration with synthetic image estimation. Magn Reson Med 2012;67:1644–1655.
17. Roujol S, Foppa M, Weingartner S, Manning WJ, Nezafat R. Adaptive registration of varying contrast-weighted images for improved tissue characterization (ARCTIC): application to T1 mapping. Magn Reson Med 2015;73:1469–1482.
18. Roujol S, Basha TA, Weingärtner S, Akçakaya M, Berg S, Manning WJ, Nezafat R. Impact of motion correction on reproducibility and spatial variability of quantitative myocardial T2 mapping. J Cardiovasc Magn Reson 2015;17:46.
19. Coniglio A, Di Renzi P, Vilches Freixas G, et al. Multiple 3D inversion recovery imaging for volume T1 mapping of the heart. Magn Reson Med 2013;69:163–170.
20. Weingärtner S, Akçakaya M, Roujol S, Basha T, Stehning C, Kissinger KV, Goddu B, Berg S, Manning WJ, Nezafat R. Free-breathing post-contrast three-dimensional T1 mapping: volumetric assessment of myocardial T1 values. Magn Reson Med 2015;73:214–222.
21. Weingärtner S, Akçakaya M, Roujol S, Basha T, Tschabrunn C, Berg S, Anter E, Nezafat R. Free-breathing combined three-dimensional phase sensitive late gadolinium enhancement and T1 mapping for myocardial tissue characterization. Magn Reson Med 2015;74:1032–1041.
22. Mehta BB, Chen X, Bilchick KC, Salerno M, Epstein FH. Accelerated and navigator-gated look-locker imaging for cardiac T1 estimation (ANGIE): development and application to T1 mapping of the right ventricle. Magn Reson Med 2015;73:150–160.
23. Chow K, Yang Y, Shaw P, Kramer CM, Salerno M. Robust free-breathing SASHA T1 mapping with high-contrast image registration. J Cardiovasc Magn Reson 2016;18:47.
24. Tsai JM, Huang TY, Tseng YS, Lin YR. Free-breathing MOLLI: application to myocardial T(1) mapping. Med Phys 2012;39:7291–7302.
25. Weingärtner S, Roujol S, Akçakaya M, Basha TA, Nezafat R. Free-breathing multislice native myocardial T1 mapping using the slice-interleaved T1 (STONE) sequence. Magn Reson Med 2014. doi: 10.1002/mrm.25387.
26. Wang X, Joseph AA, Kalentev O, Merboldt KD, Voit D, Roeloffs VB, van Zalk M, Frahm J. High-resolution myocardial T1 mapping using single-shot inversion recovery fast low-angle shot MRI with radial undersampling and iterative reconstruction. Br J Radiol 2016;89: 20160255.
27. Chen X, Mehta BB, Salerno M, Epstein FH. High Resolution Myocardial T1 Mapping Using MOLLI with Parallel Imaging and Compressed Sensing. In Proceedings of the 21st Annual Meeting of ISMRM, Salt Lake City, Utah, USA, 2013. p. 1407.
28. Larkman DJ, Hajnal JV, Herlihy AH, Coutts GA, Young IR, Ehnholm G. Use of multicoil arrays for separation of signal from multiple slices simultaneously excited. J Magn Reson Imaging 2001;13:313–317.
29. Breuer FA, Blaimer M, Heidemann RM, Mueller MF, Griswold MA, Jakob PM. Controlled aliasing in parallel imaging results in higher acceleration (CAIPIRINHA) for multi-slice imaging. Magn Reson Med 2005;53:684–691.
30. Muller S. Multifrequency selective RF pulses for multislice MR imaging. Magn Reson Med 1988;6:364–371.
31. Xu J, Moeller S, Auerbach EJ, Strupp J, Smith SM, Feinberg DA, Yacoub E, Ugurbil K. Evaluation of slice accelerations using multiband echo planar imaging at 3 T. Neuroimage 2013;83:991–1001.
32. Ugurbil K, Xu J, Auerbach EJ, et al. Pushing spatial and temporal resolution for functional and diffusion MRI in the Human Connectome Project. Neuroimage 2013;80:80–104.
33. Stab D, Wech T, Breuer FA, Weng AM, Ritter CO, Hahn D, Kostler H. High resolution myocardial first-pass perfusion imaging with extended anatomic coverage. J Magn Reson Imaging 2014;39:1575–1587.
34. Wang H, Adluru G, Chen L, Kholmovski EG, Bangerter NK, DiBella EV. Radial simultaneous multi-slice CAIPI for ungated myocardial perfusion. Magn Reson Imaging 2016;34:1329–1336.
35. Stab D, Ritter CO, Breuer FA, Weng AM, Hahn D, Kostler H. CAIPIRINHA accelerated SSFP imaging. Magn Reson Med 2011;65:157–164.
36. Schmitter S, Moeller S, Wu X, Auerbach EJ, Metzger GJ, Van de Moortele PF, Ugurbil K. Simultaneous multislice imaging in dynamic cardiac MRI at 7T using parallel transmission. Magn Reson Med 2017;77:1010–1020.
37. Weingärtner S, Akçakaya M, Basha T, Kissinger KV, Goddu B, Berg S, Manning WJ, Nezafat R. Combined saturation/inversion recovery sequences for improved evaluation of scar and diffuse fibrosis in patients with arrhythmia or heart rate variability. Magn Reson Med 2014;71:1024–1034.
38. Wong E. Optimized Phase Schedules for Minimizing Peak RF Power in Simultaneous Multi-slice RF Excitation Pulses. In Proceedings of the 20th Annual Meeting of ISMRM, Melbourne, Victoria, Australia, 2012. p. 2209.
39. Auerbach EJ, Xu J, Yacoub E, Moeller S, Ugurbil K. Multiband accelerated spin-echo echo planar imaging with reduced peak RF power using time-shifted RF pulses. Magn Reson Med 2013;69:1261–1267.
40. Kellman P, Herzka DA, Hansen MS. Adiabatic inversion pulses for myocardial T1 mapping. Magn Reson Med 2014;71:1428–1434.
41. Weingärtner S, Meßner NM, Budjan J, Lossnitzer D, Mattler U, Papavassiliu T, Zöllner FG, Schad LR. Myocardial T1-mapping at 3T using saturation-recovery: reference values, precision and comparison with MOLLI. J Cardiovasc Magn Reson 2016;18:84.
42. Setsompop K, Gagoski BA, Polimeni JR, Witzel T, Wedeen VJ, Wald LL. Blipped-controlled aliasing in parallel imaging for simultaneous multislice echo planar imaging with reduced g-factor penalty. Magn Reson Med 2012;67:1210–1224.
43. Griswold MA, Jakob PM, Heidemann RM, Nittka M, Jellus V, Wang J, Kiefer B, Haase A. Generalized autocalibrating partially parallel acquisitions (GRAPPA). Magn Reson Med 2002;47:1202–1210.
44. Pruessmann KP, Weiger M, Bornert P, Boesiger P. Advances in sensitivity encoding with arbitrary k-space trajectories. Magn Reson Med 2001;46:638–651.
45. Pruessmann KP, Weiger M, Scheidegger MB, Boesiger P. SENSE: sensitivity encoding for fast MRI. Magn Reson Med 1999;42:952–962.
46. Lakkadi N, Rosen M, Bolan PJ. Design of a Phantom for Multiparametric Quantitative MR Imaging and Spectroscopy. In Proceedings of the 23rd Annual Meeting of ISMRM, Toronto, Ontario, Canada, 2015. p. 4285.
47. Cerqueira MD, Weissman NJ, Dilsizian V, et al. Standardized myocardial segmentation and nomenclature for tomographic imaging of the heart. A statement for healthcare professionals from the Cardiac Imaging Committee of the Council on Clinical Cardiology of the American Heart Association. Circulation 2002;105:539–542.
48. Messroghli DR, Radjenovic A, Kozerke S, Higgins DM, Sivananthan MU, Ridgway JP. Modified Look-Locker inversion recovery (MOLLI) for high-resolution T1 mapping of the heart. Magn Reson Med 2004; 52:141–146.
49. Shao J, Rapacchi S, Nguyen KL, Hu P. Myocardial T1 mapping at 3.0 Tesla using an inversion recovery spoiled gradient echo readout and bloch equation simulation with slice profile correction (BLESSPC) T1 estimation algorithm. J Magn Reson Imaging 2016;43:414–425.
50. Gensler D, Morchel P, Fidler F, Ritter O, Quick HH, Ladd ME, Bauer WR, Ertl G, Jakob PM, Nordbeck P. Myocardial T1: quantification by using an ECG-triggered radial single-shot inversion-recovery MR imaging sequence. Radiology 2015;274:879–887.
51. Higgins DM, Ridgway JP, Radjenovic A, Sivananthan UM, Smith MA. T1 measurement using a short acquisition period for quantitative cardiac applications. Med Phys 2005;32:1738–1746.
52. Jang J, Bellm S, Roujol S, Basha TA, Nezafat M, Kato S, Weingartner S, Nezafat R. Comparison of spoiled gradient echo and steady-state free-precession imaging for native myocardial T1 mapping using the slice-interleaved T1 mapping (STONE) sequence. NMR Biomed 2016; 29:1486–1496.
53. Barth M, Breuer F, Koopmans PJ, Norris DG, Poser BA. Simultaneous multislice (SMS) imaging techniques. Magn Reson Med 2016;75:63–81.
54. Roujol S, Weingartner S, Foppa M, Chow K, Kawaji K, Ngo LH, Kellman P, Manning WJ, Thompson RB, Nezafat R. Accuracy, precision, and reproducibility of four T1 mapping sequences: a head-to-head comparison of MOLLI, ShMOLLI, SASHA, and SAPPHIRE. Radiology 2014;272:683–689.
55. Weingärtner S, Messner NM, Zollner FG, Akçakaya M, Schad LR. Black-blood native T1 mapping: blood signal suppression for reduced partial voluming in the myocardium. Magn Reson Med 2016. doi: 10.1002/mrm.26378.

56. Chow K, Flewitt JA, Green JD, Pagano JJ, Friedrich MG, Thompson RB. Saturation recovery single-shot acquisition (SASHA) for myocardial T(1) mapping. Magn Reson Med 2014;71:2082–2095.
57. Piechnik SK, Ferreira VM, Dall'Armellina E, Cochlin LE, Greiser A, Neubauer S, Robson MD. Shortened modified Look-Locker inversion recovery (ShMOLLI) for clinical myocardial T1-mapping at 1.5 and 3 T within a 9 heartbeat breathhold. J Cardiovasc Magn Reson 2010;12:69.
58. Kellman P, Wilson JR, Xue H, Ugander M, Arai AE. Extracellular volume fraction mapping in the myocardium, part 1: evaluation of an automated method. J Cardiovasc Magn Reson 2012;14:63.
59. Shao J, Rashid S, Renella P, Nguyen KL, Hu P. Myocardial T1 mapping for patients with implanted cardiac devices using wideband inversion recovery spoiled gradient echo readout. Magn Reson Med 2017;77:1495–1504.

SUPPORTING INFORMATION

Additional Supporting Information may be found in the online version of this article.

Fig. S1. Spatial variability in the MB T_1 maps reconstructed with Tikhonov-regularized CG-SENSE using different values for the regularization parameter. Example images of the mid-ventricular slice are provided for one volunteer at four different parameter values. Minimum spatial variability is observed at 0.05. Lower regularization parameters cause noise-induced spatial inhomogeneity, whereas higher values lead to residual leakage artifacts (white arrows).

Fig. S2. SB and MB T_1 maps acquired in six healthy subjects. MB data were reconstructed using slice GRAPPA. Visually comparable T_1 map quality with largely homogeneous myocardial T_1 and clear delineation toward the blood-pools can be observed with both T_1 mapping sequences. Slightly increased spatial inhomogeneity is observed in the MB T_1 maps.